

# Electrochemical Co-deposition of Sol–Gel/Metal Thin Nanocomposite Films

Reut Toledano, Ronen Shacham, David Avnir, and Daniel Mandler\*

*Institute of Chemistry, The Hebrew University of Jerusalem, Jerusalem 91904, Israel*

*Received January 1, 2008. Revised Manuscript Received May 8, 2008*

A single-step method for the preparation of thin sol–gel/copper mixed films is described, which is based on a novel electrochemical sol–gel methodology, resulting in nanocomposite coating. The method combines electrochemistry with the acceleration of sol–gel hydrolysis and condensation processes. While sol–gel is deposited as a result of increasing the pH in the vicinity of the electrode surface, copper ions are electrochemically reduced. Characterization of the deposited films was accomplished by scanning electron microscopy, X-ray photoelectron spectroscopy, tunneling atomic force microscopy, and other surface techniques. The different parameters that affect the structure and composition of the deposited films have been examined. We found that the morphology and grain size of the films are strongly affected by the ratio between the sol–gel monomer and copper ions. Furthermore, the potential of deposition affects also the composition of the films as it controls the kinetics of sol–gel and copper deposition.

## Introduction

Nanocomposites are commonly defined as materials consisting of two or more dissimilar materials with well-defined interfaces, where at least one of the materials being nanostructured in one, two, or three dimensions.<sup>1</sup> Composite materials made of metal particles dispersed in a dielectric matrix are of great interest and have been widely studied for their optical,<sup>2</sup> electrical,<sup>3</sup> and magnetic properties.<sup>4,5</sup> Many interesting physical phenomena have been observed and studied in these materials, such as optical nonlinearity and superparamagnetism.<sup>6</sup> Among the metal particles, copper, silver, and gold are particularly interesting for their enhanced third-order nonlinear susceptibility. The chemical and physical properties of metal/polymer composites are very sensitive to small changes in the amount, size, and shape of the metal particles. This sensitivity leads to drastic changes in the electrical and optical properties of the material, which can thus be used as sensors or switching devices. The internal, nanoscopic structure of these materials depends on the chemical nature of the components, their interactions, and the method of preparation.<sup>7,8</sup>

Nanocomposite materials are characterized by at least one phase, which is in the nanometric domain. This phase is often made of nanoparticles. The latter tend to spontaneously aggregate because of their high surface free energy. Polymers

are excellent candidates as a matrix for stabilizing nanoparticles, allowing fine control of the growth and processability of the nanocomposite.

One of the most appealing polymer technologies for fabricating nanocomposites is sol–gel. With respect to other techniques, such as high-temperature glass fusion,<sup>9</sup> ion implantation,<sup>10</sup> ion exchange,<sup>11</sup> sputtering,<sup>12</sup> etc., the sol–gel method offers a unique approach for preparing nanocomposites in a pure or organically modified sol–gel matrix.<sup>13–19</sup> There have been quite a number of reports dealing with the incorporation of nanoparticles, mostly gold, into sol–gel films.<sup>20–40</sup> Reviewing these studies suggests that there are

\* To whom correspondence should be addressed. E-mail: mandler@vms.huji.ac.il. Fax: 972 2 6585319. Tel.: 972 2 6585831.

- (1) Pomogailo, A. D. *Inorg. Mater.* **2005**, *41*, S47.
- (2) Dalacu, D.; Martinu, L. *J. Appl. Phys.* **2000**, *87*, 228.
- (3) Pakhomov, A. B.; Wong, S. K.; Yan, X.; Zhang, X. *Phys. Rev.* **1998**, *B58*, R13375.
- (4) Cintora-Gonzales, O.; Muller, D.; Estournes, C.; Richard-Plouet, M.; Poinot, R.; Grob, J.; Guille, J. *Nucl. Instrum. Methods* **2001**, *B 178*, 144.
- (5) Brouers, F.; Granovsky, A.; Sarychev, A.; Kalitsov, A. *Physica A* **1997**, *241*, 284.
- (6) Zhou, J. I.; Li, L.; Zhang, X. *Ferroelectrics* **1997**, *196*, 85.
- (7) Viart, N.; Richard-plouet, M.; Muller, D.; Pourroy, G. *Thin Solid Films* **2003**, *437*, 1.

- (8) Schurmann, U.; Takele, H.; Zaporojtchenko, V.; Faupel, F. *Thin Solid Films* **2006**, *515*, 801.
- (9) Finnigan, B.; Martin, D.; Halley, P.; Truss, R.; Campbell, K. *Polymer* **2004**, *45*, 2249.
- (10) Meldrum, A.; Boatner, L. A.; White, C. W. *Nucl. Instrum. Methods Phys. Res. B* **2001**, *178*, 7.
- (11) Jeon, H. G.; Jung, H. T.; Lee, S. W.; Hudson, S. D. *Polym. Bull.* **1998**, *41*, 107.
- (12) Musil, J.; Leipner, I.; Kolega, M. *Surf. Coat. Technol.* **1999**, *32*, 115.
- (13) Gacoin, T.; Chaput, F.; Boilot, J. P. *Chem. Mater.* **1993**, *5*, 363.
- (14) Akbarian, F.; Dunn, B. S.; Zink, J. I. *J. Raman Spectrosc.* **1996**, *27*, 775.
- (15) Kutsch, B.; Lyon, O.; Schmitt, M.; Mennig, M.; Schmidt, H. *J. Non Cryst. Solids* **1997**, *217*, 143.
- (16) Yazawa, T.; Kadono, K.; Tanaka, H.; Sakaguchi, T.; Tsubota, S.; Kuraoka, K.; Miya, M.; De-Xian, W. *J. Non-Cryst. Solids* **1994**, *170*, 105.
- (17) Gacoin, T.; Chaput, F.; Boilot, J. P.; Jaskierowicz, G. *Chem. Mater.* **1993**, *5*, 1150.
- (18) Mennig, M.; Schmitt, M.; Becker, U.; Jung, G.; Schmidt, H. *Sol-Gel Optics III* **1994**, *130*, 2288.
- (19) Wang, J.; Pamidi, P. V. A. *Anal. Chem.* **1997**, *69*, 4490.
- (20) Bharathi, S.; Lev, O. *Chem. Commun.* **1997**, 2303.
- (21) Bharathi, S.; Lev, O. *Anal. Commun.* **1998**, *35*, 29.
- (22) Selvan, S. T.; Nogami, M.; Nakamura, A.; Hamanaka, Y. *J. Non-Cryst. Solids* **1999**, *255*, 254.
- (23) Lee, B.; Zhu, H. G.; Zhang, Z. T.; Overbury, S. H.; Dai, S. *Microporous Mesoporous Mater.* **2004**, *70*, 71.
- (24) Fukushima, M.; Yanagi, H.; Hayashi, S.; Suganuma, N.; Taniguchi, Y. *Thin Solid Films* **2003**, *438*, 3.
- (25) Wu, Z. S.; Li, J. S.; Lou, M. H.; Shen, G. L.; Yu, R. Q. *Anal. Chim. Acta* **2005**, *528*, 235.

basically three approaches for the formation of nanoparticles-encapsulated sol–gel films. The first studies conducted by Lev and co-worker<sup>20,21</sup> involved the reduction of  $\text{AuCl}_4^-$  in the presence of a sol–gel monomer having an amino group that stabilized the gold nanoparticles. This approach has been adopted by others<sup>22–24</sup> who used other protocols for reducing the gold ions, such as tetraalkyl phosphonium ions and photochemistry. A second concept demonstrated by Shen and co-workers,<sup>25</sup> Dong and co-workers,<sup>26</sup> and Wilson and co-worker<sup>27</sup> comprised the formation of first a sol–gel film having alkanethiol moieties, using usually mercaptopropyltrimethoxysilane, which was further immersed in gold nanoparticles solution. The latter was extracted by the thiol groups. The third method developed by Liz-Marzán and co-workers<sup>28</sup> and Lu et al.<sup>29</sup> is based on coating gold nanoparticles by a sol–gel film. Fine control of the amount of the alkoxides, water, ethanol, and ammonia was used to prevent gel formation.

Sol–gel films are usually formed by three alternative methods: spin coating,<sup>41–43</sup> dip coating,<sup>44,45</sup> and spraying.<sup>46–49</sup> Although these methods are straightforward and simple to apply, two of them, i.e., dip and spin coating, can be applied to flat surfaces only, where spraying can be used for coating complex geometries. Moreover, partial coating of surfaces, namely, coating of a certain pattern, is impossible without application of a mask.<sup>50</sup> Recently, we reported a novel

approach for sol–gel deposition based on electrochemical enhancement of the rate of condensation.<sup>51</sup> Applying either a negative or positive potential caused solvent reduction or oxidation, respectively, which altered the pH on the electrode surface.

Here, we describe further advancement of this approach where sol–gel/metal nanocomposites are prepared in a single electrochemical step. Specifically, the formation of thin nanocomposite films made of copper–silica or copper–titania are demonstrated. We show that introduction of  $\text{Cu}^{2+}$  ions to the deposition solution generates, along with the electrodeposition of the film, metallic copper, resulting in the formation of the nanocomposites  $\text{Cu}/\text{SiO}_2$  or  $\text{Cu}/\text{TiO}_2$ . The nanocomposites were characterized by a number of surface techniques including high-resolution scanning electron microscopy, scanning tunneling atomic force microscopy, and X-ray photoelectron spectroscopy. We find that the applied potential, as well as the ratio between the  $\text{Cu}^{2+}$  and the sol–gel monomer, greatly affect the size and morphology of the copper nanoparticles embedded in the sol–gel matrix.

## Experimental Section

**Instrumentation.** Electrochemical experiments were performed with a VersaStat potentiostat (EG&G) using a standard three-electrode cell with Ag/AgBr as a reference electrode and a 6 mm diameter graphite rod as a counter electrode. The working electrodes were indium tin oxide (ITO) on glass ( $R_S = 15\text{--}25\ \Omega$ , Delta Technologies Stillwater, MN), thin gold films (ca. 200 nm) deposited on glass that were previously covered with a thin (ca. 5 nm) chromium layer, or stainless steel 316L plates. A homemade lifter was used to withdraw the substrates from the deposition solutions at a rate of ca.  $50\ \mu\text{m}\cdot\text{s}^{-1}$ , with constant application of the potential and with slow stirring. The interfacial capacity was measured using an AutoLab potentiostat (PGSTAT 30, EcoChemie, Utrecht, The Netherlands).

SEM images were acquired by a JEOL JSM-6400 scanning microscope with an electron-beam intensity of 5 keV, unless otherwise written. Analysis of the elements was performed with SEM equipped with energy-dispersive X-ray analysis (EDX). The thickness of the deposited films was measured with a profilometer (P-15, KLA-Tencor Co., San Jose, CA). Scanning tunneling atomic force microscope (TUNA) measurements were conducted using a Nanoscope Dimension 3100 scanning probe microscope with a Nanoscope IVa controller (probe MESP, Veeco). X-ray photoelectron spectroscopy (XPS) was used for chemical analysis of the film surface. An Axis Ultra spectrometer (Kratos Analytical, Manchester UK) was used with Mg  $K\alpha$  radiation of 1486.71 eV. Data were collected and analyzed by a vision processing program.

**Chemicals.** Tetramethoxysilane (TMOS), phenyltrimethoxysilane (PTMOS), and titanium tetra-*n*-propoxide ( $\text{Ti}(\text{OPr})_4$ ) were purchased from Aldrich (98% purity) and used as-received. Absolute ethanol and dry 2-propanol (A.R, Frutarom), extra-pure  $\text{KNO}_3$  (Merck),  $\text{LiClO}_4$  and  $\text{CuCl}_2$  (Aldrich), potassium hydrogen phthalate (BDH Laboratory), HCl (J.T. Baker), and deionized water (EasyPure UV, Barnstead) were used for preparing the different solutions.

**Procedures.** The electrodes, i.e., ITO plates, thin gold films, or stainless steel 316L plates, were washed prior to film deposition with water, ethanol, and water again, followed by drying at room temperature for 1–2 h. The solution for the electrodeposition of silica-based sol–gel films consisted of 1.25 mL of TMOS, 5 mL

- (26) Jia, J. B.; Wang, B. Q.; Wu, A. G.; Cheng, G. J.; Li, Z.; Dong, S. J. *Anal. Chem.* **2002**, *74*, 2217.
- (27) Chen, X. H.; Wilson, G. S. *Langmuir* **2004**, *20*, 8762.
- (28) Kobayashi, Y.; Correa-Duarte, M. A.; Liz-Marzan, L. M. *Langmuir* **2001**, *17*, 6375.
- (29) Lu, Y.; Yin, Y. D.; Li, Z. Y.; Xia, Y. A. *Nano Lett.* **2002**, *2*, 785.
- (30) Wu, Z. S.; Li, J. S.; Luo, M. H.; Shen, G. L.; Yu, R. Q. *Anal. Chim. Acta* **2005**, *528*, 235.
- (31) Lei, C. X.; Yang, Y.; Wang, H.; Shen, G. L.; Yu, R. Q. *Anal. Chim. Acta* **2004**, *513*, 379.
- (32) Shukla, S.; Seal, S. *Nanostruct. Mater.* **1999**, *11*, 1181.
- (33) Epifani, M.; Giannini, C.; Tapfer, L.; Vasanelli, L. *J. Am. Ceram. Soc.* **2000**, *83*, 2385.
- (34) Kozuka, H.; Okuno, M.; Yoko, T. *J. Ceram. Soc. Jpn.* **1995**, *103*, 1305.
- (35) Livage, J. *Bull. Mater. Sci.* **1999**, *22*, 201.
- (36) Selvan, S. T.; Nogami, M.; Nakamura, A.; Hamanaka, Y. *J. Non-Cryst. Solids* **1999**, *255*, 254.
- (37) Epifani, M.; Giannini, C.; Tapfer, L.; Vasanelli, L. *J. Am. Ceram. Soc.* **2000**, *83*, 2385.
- (38) Kobayashi, Y.; Correa-Duarte, M. A.; Liz-Marzan, L. M. *Langmuir* **2001**, *17*, 6375.
- (39) Pol, V. G.; Gedanken, A.; Calderon-Moreno, J. *Chem. Mater.* **2003**, *15*, 1111.
- (40) Mine, E.; Yamada, A.; Kobayashi, Y.; Konno, M.; Liz-Marzan, L. M. *J. Colloid Interface Sci.* **2003**, *264*, 385.
- (41) Petit-Dominguez, M. D.; Shen, H.; Heineman, W. R.; Seliskar, C. J. *Anal. Chem.* **1997**, *69*, 703.
- (42) Li, Y.; Pan, Q. Y.; Zhang, J. P.; Cheng, Z. X.; Chen, H. H. *Wuji Cailiao Xuebao* **2004**, *19*, 1065.
- (43) Vorotilov, K.; Petrovsky, V.; Vasiljev, V. *J. Sol-Gel Sci. Technol.* **1995**, *5*, 173.
- (44) Brinker, C. J.; Frye, G. C.; Hurd, A. J.; Ashley, C. S. *Thin Solid Films* **1991**, *201*, 97.
- (45) Xu, A. W.; Yu, J. C.; Zhang, H. X.; Zhang, L. Z.; Kuang, D. B.; Fang, Y. P. *Langmuir* **2002**, *18*, 9570.
- (46) Giampaolo Conde, A. R.; Puerta, M.; Ruiz, H.; Lira Olivares, J. J. *Non-Cryst. Solids* **1992**, *467*, 147.
- (47) Puetz, J.; Aegerter, M. A. *Glass Sci. Technol.* **2004**, *77*, 229.
- (48) Puetz, J.; Gasparro, G.; Aegerter, M. A. *Thin Solid Films* **2003**, *442*, 40.
- (49) Schottner, G.; Kron, J.; Deichmann, A. *J. Sol-Gel Sci. Technol.* **1998**, *13*, 183.
- (50) Walcarius, A.; Mandler, D.; Cox, J. A.; Collinson, M.; Lev, O. J. *Mater. Chem.* **2005**, *15*, 3363.

(51) Shacham, R.; Avnir, D.; Mandler, D. *Adv. Mater.* **1999**, *11*, 384.

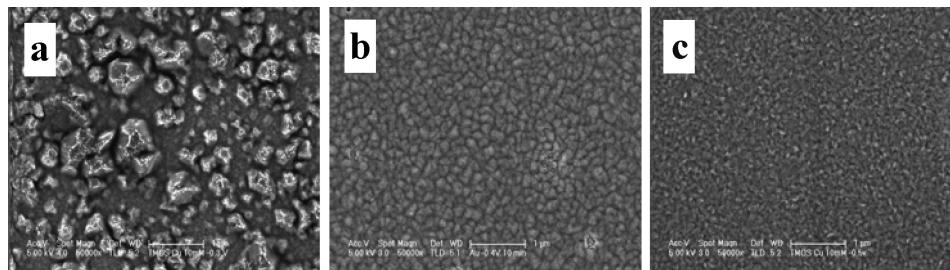


**Figure 1.** SEM images (the bar indicates 1  $\mu\text{m}$ ) of Cu/SiO<sub>2</sub> electrodeposited films (10 mM CuCl<sub>2</sub>) as a result of application of different negative potentials: (a)  $-0.3$  V, (b)  $-0.4$  V, and (c)  $-0.5$  V for 10 min.

of 0.2 M KNO<sub>3</sub>, and phthalate buffer (1 mM, pH = 3.5). Titania-based sol-gel films were electrochemically deposited in a solution containing 0.2 M Ti(OPr)<sub>4</sub>, 8.9 mM water, and 0.1 M LiClO<sub>4</sub> in dry 2-propanol. Hydrolysis was carried out by stirring the above-described solutions for 1 h at room temperature. Cupric ions (1–10 mM) were added to the solutions at this stage. Then the electrodes were placed in the electrochemical cell and the working electrode was mounted on the lifter. Usually, a cyclic voltammetry was carried out prior to chronoamperometry. A constant negative potential (between  $-0.3$  and  $-1.4$  V vs Ag/AgBr) was applied to the electrode for 1–10 min under continuous stirring. The current as a function of time was recorded. After this period, the electrode was slowly withdrawn using the lifter while the potential was still applied. The electrode was dried in air for 24 h before further characterization was performed. Profiles of the deposited sol-gel nanocomposite films were recorded across a notch that was manually scratched by a wooden stick.

## Results and Discussion

The first study where sol-gel was electrochemically deposited was reported by Shacham et al.<sup>51</sup> who proposed a new approach for sol-gel film formation. The method involved the electrochemical control of the pH near a conductive surface by solvent reduction or oxidation. Furthermore, the approach was based on the “two-step” sol-gel preparation procedure in which the hydrolysis of a metal alkoxide is carried out initially at a low pH, followed by polycondensation of the hydrolyzed monomer at a higher pH. According to this methodology, applying either negative or positive potentials to a conducting substrate alters the pH at the electrode surface, which catalyzes the polymerization of sol-gel monomers, leading to the deposition of the appropriate oxide film. Here, we expand this approach to depositing sol-gel/metal nanocomposites by the simultaneous reduction of metal ions, e.g., Cu<sup>2+</sup>, and the solvent, such as water, resulting in the co-deposition of metal and sol-gel.

Initially, copper/silica films were electrochemically codeposited by applying a negative potential to a gold surface. Figure 1a–c shows SEM images of films that were deposited upon application of negative potentials (between  $-0.3$  and  $-0.5$  V) in the presence of 10 mM CuCl<sub>2</sub>. EDX analysis confirmed that the deposits are made of copper and the area between the deposits contains mostly silica. Moreover, it is evident that the applied potential strongly affects the morphology and grain size of the deposited copper. As the applied potential was more negative, the average size of the grains decreased and their density increased. It should

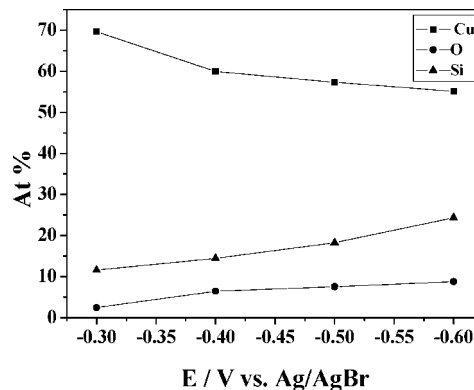


**Figure 2.** Atomic percent of copper, silicon, and oxygen in the deposited films as a function of the applied potential. The concentration of Cu<sup>2+</sup> in the deposition solution was 10 mM and time of deposition 10 min.

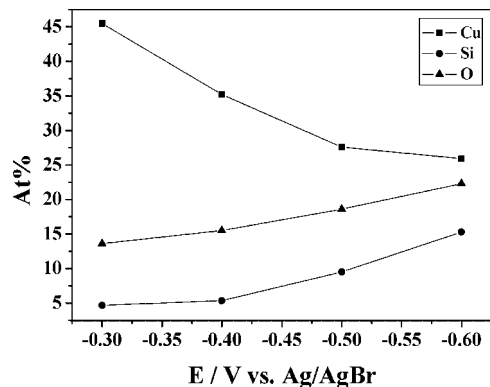
be mentioned that deposition can also be driven, in principle, by the electric field, that is, by an electrophoretic mechanism. Yet, this usually requires very high potentials or relatively low ionic strength. Therefore, we do not believe that migration contributes significantly to the overall deposition under our experimental conditions. The average grain size (calculated by ImageJ software) of the particles formed at  $-0.3$  and  $-0.4$  V was  $1.2 \times 10^5$  and  $6 \times 10^3$  nm<sup>2</sup>, respectively. These observations are in accordance with previous studies of co-deposition of metals in the presence of polymers.<sup>52,53</sup> The effect of the potential on the density of the deposits can be interpreted based on a nucleation and growth mechanism.<sup>54</sup> A more negative potential facilitates the formation of nucleation sites and therefore reduces the size of the average nuclei. The number of active nucleation sites should be proportional to the applied potential, which reduces the nucleation energy barrier.

Figure 2 displays the atomic percent of the elements, i.e., copper, silicon, and oxygen in the film (obtained from EDX analysis) as a function of the applied potential (the total atomic percentage sums to less than 100% because two other elements, namely, Au and C, were omitted). The analysis was made on a relatively large area (approximately  $100 \times 100$   $\mu\text{m}$ ) that included many grains. Furthermore, the same trend was found in each spot that was analyzed. It can be seen that as the applied potential was more negative, the amount of the deposited copper decreased and, at the same

(52) Kao, W. H.; Kuwana, T. *J. Am. Chem. Soc.* **1984**, *106*, 473.

(53) Kost, K. M.; Bartak, D. E.; Kazee, B.; Kuwana, T. *Anal. Chem.* **1988**, *60*, 2379.

(54) Zhou, X. J.; Harmer, A. J.; Heinig, N. F.; Leung, K. T. *Langmuir* **2004**, *20*, 5109.



**Figure 3.** Same as Figure 2 but the concentration of cupric ions in the deposition solution was 1 mM.

time, the content of silicon and oxygen increased respectively. The percentage of Cu varied between 55 and 70%, implying that most of the film was made of metal. The oxidation state of the copper cannot be determined from these measurements and will be discussed later.

Shifting the potential to negative values should affect the heterogeneous kinetics of both the reduction of copper and that of the solvent. We have shown<sup>55</sup> that in water/alcohol mixtures and under the potentials applied, water reduction dominates. Evidently, the reduction of cupric ions commences at more positive potentials than the reduction of protons. Hence, we expect that at less negative potentials the kinetics of cupric ions reduction will be more facile than that of protons. Shifting the potentials more negative will eventually result in the diffusion-controlled reduction of cupric ions, while increasing the rate of proton reduction. The latter will cause a local increase of the pH near the electrode surface and the massive deposition of sol–gel.

Another factor which affects the morphology and composition of the deposited films is the concentration of the metal ions in the deposition solution. In essence, as the concentration of  $\text{Cu}^{2+}$  decreases, the percentage of copper in the film as well as its average grain size decrease, *vide infra*. In addition, the potential has the same effect as shown above (Figure 1); namely, smaller grains were obtained at more negative potentials. Figure 3 shows the atomic percent of the various elements in a film deposited from a solution containing 1 mM  $\text{CuCl}_2$  as a function of the applied potential. It is evident that the changes in the element percentage are similar to those measured at higher  $\text{Cu}^{2+}$  concentration (in the deposition solution). However, the Cu percentage falls more rapidly and the element percentage of Si and O increases more steeply than those in a more  $\text{Cu}^{2+}$  concentrated solution. This is expected due to the effect of the initial  $\text{Cu}^{2+}$  concentration on the gradient profile and the flux of the ions approaching and depositing onto the electrode surface.

The effect of the metal ion concentration in the deposition solution on the morphology of the deposited films is more obvious upon deposition of the composite film on an indium tin oxide (ITO) electrode (Figure 4). The SEM images clearly show that as the concentration of  $\text{Cu}^{2+}$  decreases, the size

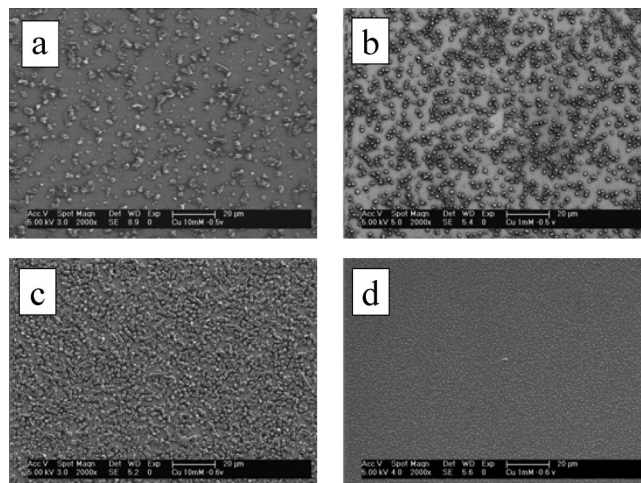


**Figure 4.** SEM images of Cu/TMOS based sol–gel nanocomposites on ITO, deposited from different  $\text{Cu}^{2+}$  concentrations [(a) and (b)  $[\text{Cu}^{2+}] = 10 \text{ mM}$ ; (c) and (d)  $[\text{Cu}^{2+}] = 1 \text{ mM}$ ] and applied potentials [(a) and (c)  $-0.5 \text{ V}$  and (b) and (d)  $-0.6 \text{ V}$ ]. Time of deposition was always 10 min.

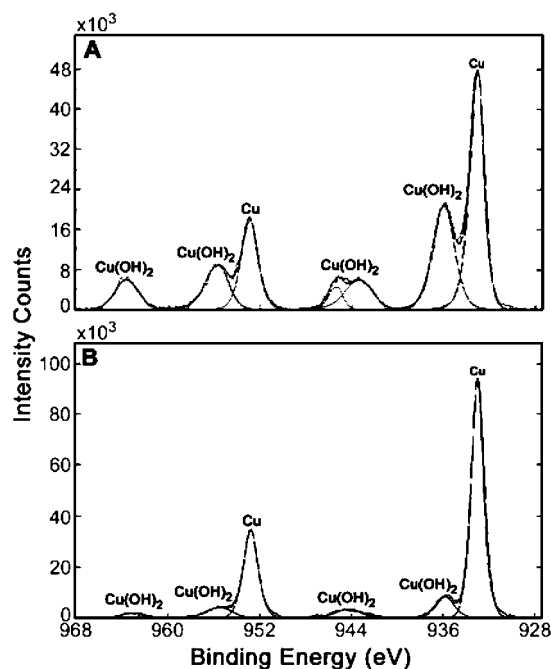


**Figure 5.** XPS spectra of the electrodeposited films at two different concentrations of cupric ions: (A) 1 mM and (B) 10 mM. A constant potential of  $-0.4 \text{ V}$  was applied for 10 min.

of the Cu deposits decreases as well independently of the applied potential. This supports our previous results suggesting that Cu is deposited under diffusion-controlled conditions, which diminishes the effect of the surface on deposition. The effect of the surface will be discussed later.

In spite of the fact that copper is the dominant component in the film, it is not obvious that  $\text{Cu}^{2+}$  ions are reduced and elemental copper is indeed deposited. A parallel route could involve the deposition of copper hydroxide or copper oxide due to the elevated pH in the vicinity of the electrode surface. Hence, X-ray photoelectron spectroscopy (XPS) was used to determine the oxidation state of copper in the deposited films (Figure 5). We were careful not to expose the samples to air to avoid the oxidation of copper. Hence, the samples

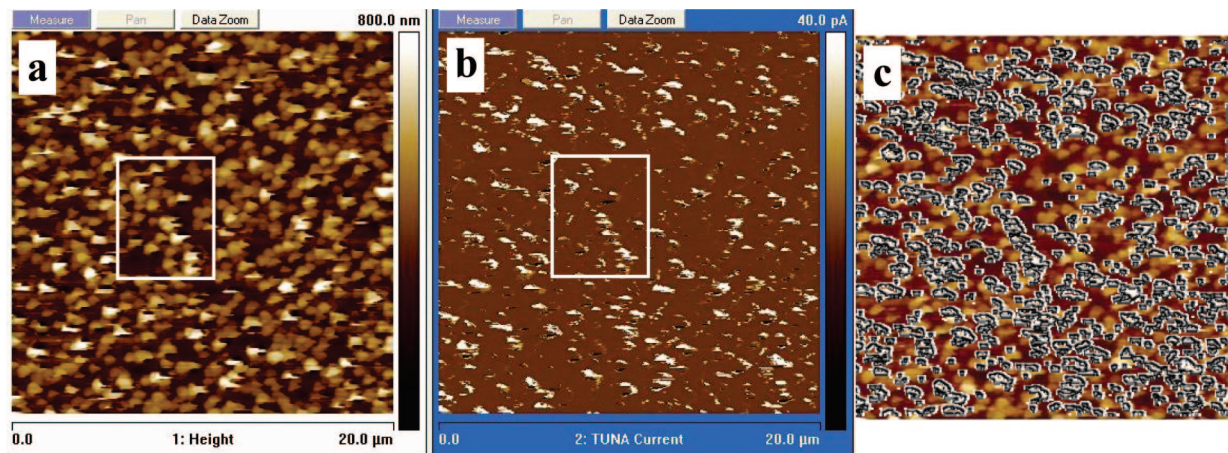


**Figure 6.** (a) Topography, (b) conductivity, and (c) topography–conductivity overlapping images obtained by TUNA of a Cu/SiO<sub>2</sub> film electrochemically deposited from 10 mM Cu<sup>2+</sup> and TMOS upon application of  $-0.6$  V for 10 min.

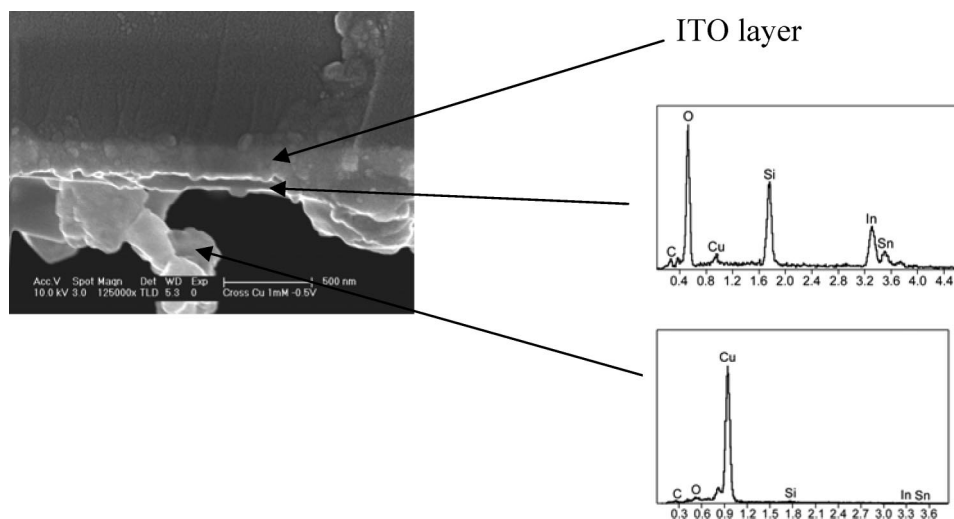


**Figure 7.** SEM image of a cross section made in a Cu/SiO<sub>2</sub> film, which was electrochemically deposited by applying  $-0.4$  V in 10 mM Cu<sup>2+</sup> and TMOS solution for 10 min. On the right, the EDX analysis of the sol–gel film and the copper grain, respectively.

were kept in a desiccator and transferred to the XPS chamber quickly prior to the measurement. XPS enables easy determination of the oxidation state of copper as compared with those of many other metals. The 2p<sub>3/2</sub> and 2p<sub>1/2</sub> XPS signals of elemental Cu, which appear at 932.7 and 952.5 eV, respectively, are well-separated from the same signals of Cu(OH)<sub>2</sub>, which appear at 935 and 955 eV, respectively. Furthermore, CuO and Cu(OH)<sub>2</sub> are always characterized by two additional shake-up lines of the Cu 2p observed in its compounds at 944 and 964 eV.<sup>56</sup>

Figure 5 shows the XPS spectra of films electrochemically deposited from 1 and 10 mM Cu<sup>2+</sup>. The presence of Cu as well as Cu(OH)<sub>2</sub> is evident in both spectra. The signals match well with the literature values mentioned above. It can be seen that increasing the Cu<sup>2+</sup> concentration in the deposition solution increases the ratio between metallic and ionic copper in the film. We found (based on the ratio between peak areas) that the ratio between copper and cupric ions increases from 1.6 to 8 as a result of increasing the concentration of Cu<sup>2+</sup> in the deposition solution from 1 to 10 mM. These results

**Table 1.** Thickness and Capacity of the TMOS/Cu Nanocomposite Films as a Function of Time of Deposition (Potential of Deposition Was  $-0.4$  V)

electrodeposition time (min)	film thickness ( $\mu\text{m}$ )	capacity (Cs/ $\mu\text{F}$ )
1	2.1	43.9
2	2.9	41.5
5	3.4	36.1
10	4.6	27.5

are understandable taking into account the higher concentration of OH<sup>-</sup> that is formed upon decreasing the concentration of Cu<sup>2+</sup>.

Tunneling atomic force microscopy (TUNA) is a scanning probe technique, which provides simultaneous conductivity and topography images with very high lateral resolution. This is an ideal technique that should clearly differentiate between the metallic conducting zones and that of the nonconducting sol–gel phase. Figure 6 shows the topography (a) and conductivity (b) of an electrochemically deposited Cu/SiO<sub>2</sub> film. To compare the two images, a small fraction of the same areas was marked. Moreover, we processed the conductivity image and left only the bright spots representing the high conducting areas. Then we overlapped the processed

(56) Moulder, J. F.; Stickle, W. F.; Sobol, P. E.; Bomben, K. D. In *Handbook of X-ray Photoelectron Spectroscopy*; Chastain, J., King, R. C., Jr., Eds.; Perkin Elmer: Eden Prairie, MN, 1992.

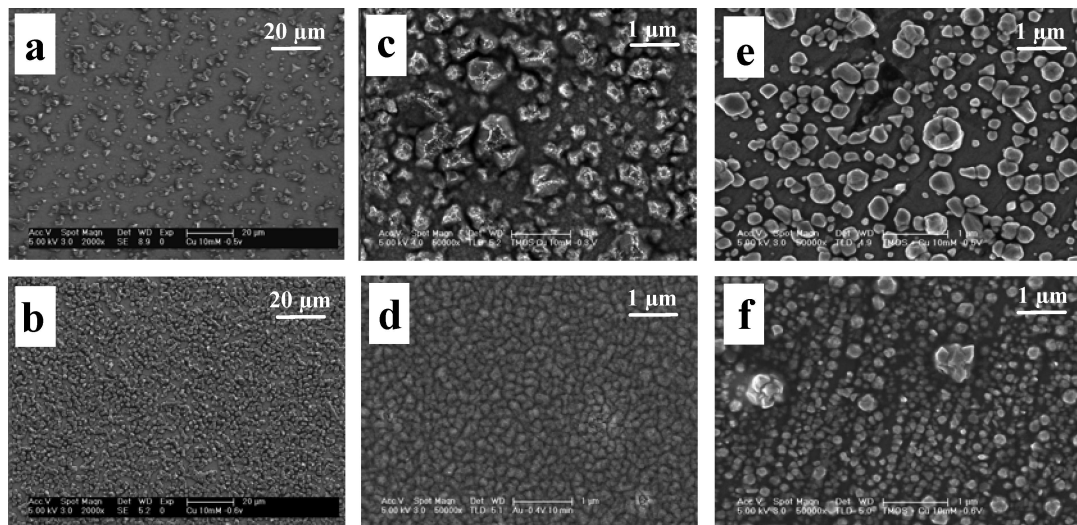


**Figure 8.** SEM images of Cu/SiO<sub>2</sub> electrodeposited film (10 mM CuCl<sub>2</sub>) upon application of negative potential for 10 min: (a,b) ITO, (c,d) Au, (e,f) stainless steel 316L. Potential of deposition: (a)  $-0.3$  V; (b)  $-0.4$  V; (c,e)  $-0.5$  V, and (d,f)  $-0.6$  V.

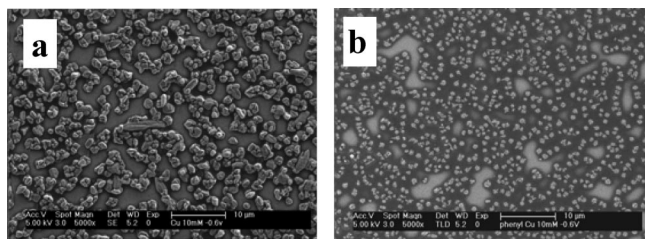


**Figure 9.** SEM images of copper/silica composites electrodeposited on ITO (10 mM CuCl<sub>2</sub>) upon application of  $-0.6$  V for 10 min: (a) TMOS-based film; (b) PhTMOS-based film.

**Table 2. Average Size of the Deposits as a Function of Potential and Nature of the Electrode**

nature of the electrode	applied potential (V)	average size of the deposits (nm <sup>2</sup> )
ITO	$-0.5$	$46.4 \times 10^5$
ITO	$-0.6$	$12.6 \times 10^5$
Au	$-0.5$	$1.2 \times 10^5$
Au	$-0.6$	$6 \times 10^3$
S.S	$-0.5$	$19.5 \times 10^3$
S.S	$-0.6$	$11.9 \times 10^3$

image with the topography image (Figure 6c). It is evident that the higher topographic areas nicely correlate with enhanced conductivity, which implies that these are made of metallic copper.

To further examine the heterogeneity of the film, a cross section was made and inspected by SEM. The image (Figure 7) shows that the ITO layer, which is approximately 1500 Å, is entirely covered by a thin layer of sol–gel in which Cu crystallites are scattered. This was confirmed by EDX analysis shown in Figure 7. Namely, the composition of the thin layer was mostly silica, whereas the major component of the grains was copper. The Cu deposits extrude from the sol–gel film up to 1 μm. It can be seen from Figure 7 that two phases were obtained on the ITO surface, the first layer consisting of mostly silica whereas the copper grains grew from the surface across it.

Measuring the capacity provides further insight into the films. Table 1 summarizes the capacity of TMOS/Cu based films, which were deposited on thin Au films at  $-0.4$  V for

different times. The measurements were carried out using alternating current voltammetry (ACV). The film thickness was also measured independently by profilometry and shows that it increases as the time of deposition increases. It can be seen that the capacity decreases with increasing the time of deposition, namely, as the film thickness increases. Trying to analyze the results based on the Helmholtz double-layer model resulted in an unreasonable value for the dielectric constant, although a linear dependence between the capacity and the reciprocal value of the thickness was obtained. This is not surprising taking into consideration the nature of the film and its growth mechanism. That is, the copper is electrochemically reduced and therefore ohmically connected to the conducting surface underneath. Therefore, the area of the capacitor needs to be corrected for the real area, which includes the copper surface. From the linear plot we obtained the real area assuming that the dielectric constant of the layer is 3, which is that of the sol–gel.<sup>57</sup> Dividing the real area by the geometric area gives the roughness factor that is equal to 34. This high roughness factor is reasonable in view of the growth mechanism and topography of the coating.

Our method of co-deposition should be fairly generic in terms of the type of surface and sol–gel monomers that can be deposited. The effect of the surface on electrodeposition was studied by employing three different surfaces, i.e., ITO, gold, and stainless steel 316L. The composition of the solution (10 mM Cu<sup>2+</sup>) and time of deposition (10 min) were identical, whereas the applied potential was determined so that the electrolysis current was approximately 200 μA. Obviously, the chosen potential was less negative for gold than ITO or stainless steel because of the faster kinetics of proton reduction as well as Cu<sup>2+</sup> reduction. Figure 8 shows SEM images of TMOS/Cu films that were electrodeposited on ITO (a–b), Au (c–d), and stainless steel (e–f). Note the difference in magnification. It can be seen that the grains of Cu deposited on ITO are larger and their density is lower than that on Au or stainless steel. These findings can be explained by the difference in the rate of Cu<sup>2+</sup> reduction on

(57) [www.clippercontrols.com/info/dielectric\\_constant.html](http://www.clippercontrols.com/info/dielectric_constant.html).

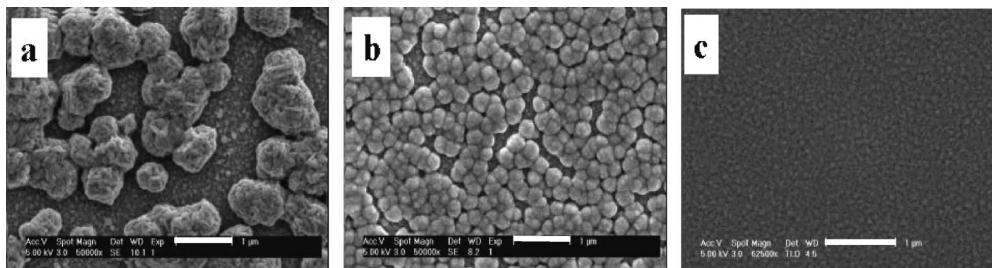


**Figure 10.** SEM images of Cu/TiO<sub>2</sub> electrodeposited films (−1.4 V). Seen are copper granules obtained at two different concentrations: (a) 100 mM and (b) 10 mM. When 1 mM of CuCl<sub>2</sub> was used, only the underlying ITO was observed.

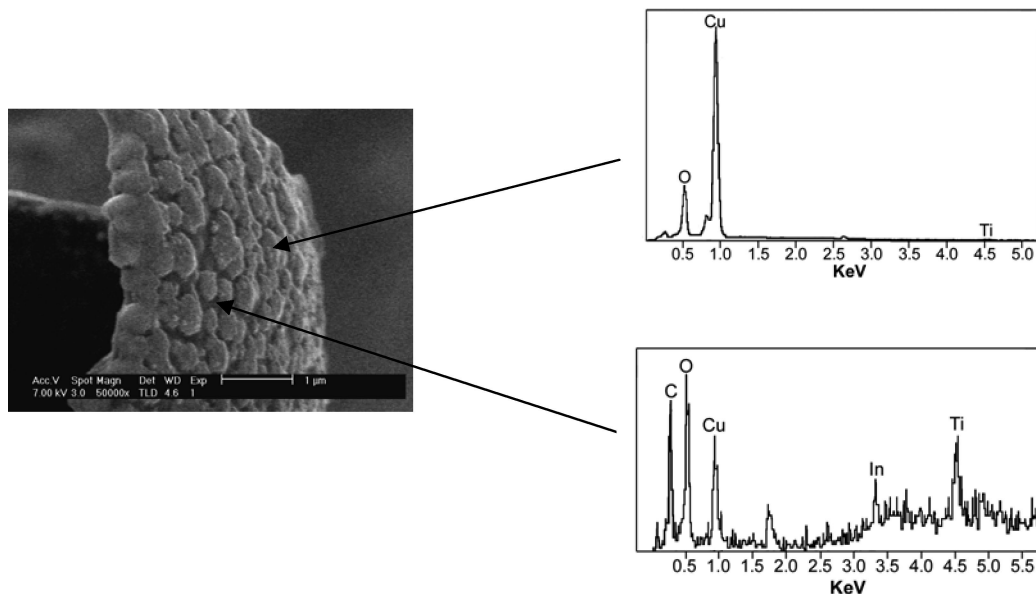


**Figure 11.** SEM image of a partially detached Cu/TiO<sub>2</sub> film electrodeposited on ITO. On the left, EDX analysis of a copper grain and the area between the grains.

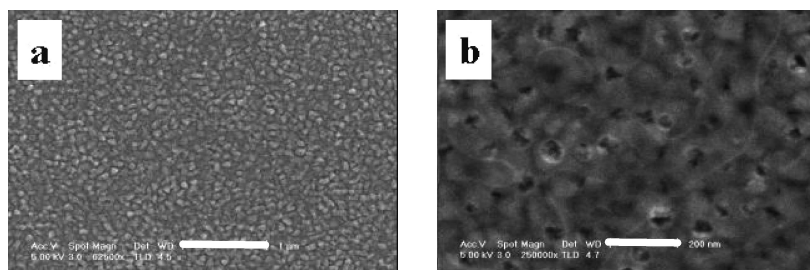


**Figure 12.** SEM images of TiO<sub>2</sub> electrodeposited films (2.0 V, 100 mM CuCl<sub>2</sub>) (a) before and (b) after application of a second potential of −1.0 V (the bars indicate 1 μm and 200 nm, respectively).

these substrates. Cu<sup>2+</sup> electrochemical reduction is more facile on a metallic surface, e.g., Au and stainless steel, than on other conducting surfaces, such as ITO and glassy carbon. The CV performed in 1 mM Cu<sup>2+</sup> in the same solution, however, in the absence of the sol–gel monomer (not shown) shows indeed that the wave of Cu<sup>2+</sup> reduction of ITO is shifted to more negative potentials than on Au or stainless steel. Therefore, the nucleation of Cu, which is faster on Au and stainless steel, results in smaller grains and higher density than that on ITO. Furthermore, the effect of potential is also inconsistent with these findings; namely, the size of the grains decreases while the density increases as the potential of deposition is made more negative, independent of the type of surface.

The generic nature of the method was further explored by co-deposition of films based on other silica monomers, such as phenyltrimethoxysilane (PhTMOS). The latter was added to the deposition solution, while the other parameters were unchanged. Figure 9 shows SEM images of TMOS/Cu and PhTMOS/Cu electrodeposited on ITO. Table 2 summarizes the average size of the deposits. It is evident that the morphology of the film and the size of the grains depend on the sol–gel monomer. This is not trivial as we recall that the grains are mainly made of Cu. It can be seen that the grains of TMOS/Cu are smaller and denser than those formed by PhTMOS/Cu. This implies that the deposition of Cu in the presence of TMOS is more facile than that with PhTMOS and therefore it nucleates and grows faster. We

attribute this difference to the hydrophobic nature of PhT-MOS, which presumably affects the kinetics of  $\text{Cu}^{2+}$  reduction on ITO.

Our method is not limited to silicon-based monomers and can be extended to other metals, such as Ti, Zr, and Al. The next section demonstrates the implementation of the electrochemical co-deposition of copper using a titanium monomer, e.g., titanium tetra-*n*-propoxide,  $\text{Ti}(\text{OPr})_4$ . A similar approach was used whereby  $\text{Cu}^{2+}$  was introduced into the deposition solution consisting of  $\text{Ti}(\text{OPr})_4$  and an electrolyte.  $\text{Cu}/\text{TiO}_2$  was electrochemically deposited onto ITO by applying constant negative or positive potentials.

Figure 10a–c shows the effects of varying the  $\text{Cu}^{2+}$  concentration (from 1 to 100 mM) on the growth morphology of the copper nanoparticles electrodeposited at  $-1.4$  V, while keeping all the other deposition parameters unchanged. Deposits can be clearly seen at the two higher concentrations. It is evident that the concentration of  $\text{Cu}^{2+}$  strongly affects the morphology and grain size of the deposited copper. A similar tendency was obtained; namely, as the concentration of  $\text{Cu}^{2+}$  in the deposition solution increased, the average size of the grains increased and their density decreased.

Figure 11 shows part of the  $\text{Cu}/\text{TiO}_2$  film, which was peeled off. Sub-micrometer size grains can be seen isolated by a thinner film. EDX of the grains and the area surrounding them are also shown (Figure 11) and indicate that the grains are made of copper, while the areas are made of primarily titania, although some copper can be found as well.

We recall that sol–gel films can also be deposited by application of positive potentials.<sup>55,58,59</sup> However, in this case copper should not be reduced. Indeed, as seen in Figure 12a, when a potential of 2.0 V was applied to ITO in the above solution (100 mM  $\text{CuCl}_2$ ), only the grains of the substrate (ITO) were observed. Nevertheless, EDX analysis clearly showed that copper ions were entrapped inside the film. Applying a negative potential to the film ( $-1.0$  V) produced a homogeneous, nonaggregated distribution of metallic copper (Figure 12b), which masks the fine grains of the ITO seen in Figure 12a.

## Conclusions

The electrochemical co-deposition of sol–gel and copper has been demonstrated. Co-deposition proceeds through the potential-induced deposition of sol–gel that is driven by affecting the concentration of protons and hydroxyl ions on the electrode surface by potential. Applying a negative potential to the electrode caused the reduction of the protic solvent and the increase of  $\text{RO}^-$  ions, which catalyze the condensation of the silica or titania monomers. Furthermore, the negative potential caused also the reduction of cupric ions present in the deposition solution. The co-deposition resulted in the formation of thin nanocomposite films. We found a significant influence of primarily two parameters, i.e., the potential of deposition and the ratio between the sol–gel monomer and the cupric ions, on the structure and morphology of the deposits. Increasing the concentration of the sol–gel monomers or shifting the deposition potentials to more negative values yields less copper in smaller and denser grains. Furthermore, this approach is highly generic and can be implemented with other sol–gel monomers (different metals as well as ligands), metal ions, and type of surfaces.

Our electrochemical co-deposition method has significant advantages as compared with other conventional procedures for preparing sol–gel coatings, such as spin coating, dip coating, and spraying. It allows coating of complex nonplanar geometries and control over the thickness and composition of the nanocomposite and assures that the metallic structures will be ohmically connected with the underlying substrate. The fact that the metallic structures formed inside the insulating matrix are ohmically connected is crucial in many applications such as catalysis, sensing, supercapacitors, and solar energy devices. Moreover, these micro- and nanostructures exhibit very high surface area, which is also important in such applications. Further experiments in which previously prepared nanoparticles are added into the sol–gel deposition solutions and electrochemically co-deposited to yield well-defined nanocomposite films are currently under investigation in our laboratory.

**Acknowledgment.** This study was supported by the Israel Ministry of Science under the Infrastructure program. The Harvey M. Krueger Family Center for Nanoscience and Nanotechnology of the Hebrew University is acknowledged.

CM800002Z

(58) Collinson, M. M.; Moore, N.; Deepa, P. N.; Kanungo, M. *Langmuir* **2003**, *19*, 7669.

(59) Sayen, S.; Walcarius, A. *Electrochem. Commun.* **2003**, *5*, 341.